Journal of
Polymer Materials

Tech Science Press

Doi:10.32604/jpm.2026.075290

ARTICLE

Study on the Adsorption Properties of Sodium Alginate-Modified Polyacrylic Acid Composite Hydrogel for Heavy Metal Cu^{2+} in Aqueous Solution

Hui Fan and Xinqiang Li*

College of Architectural Engineering, Anhui University of Applied Technology, Hefei, 230011, China

*Corresponding Author: Xinqiang Li. Email: lixinqiang@uta.edu.cn

Received: 29 October 2025; Accepted: 30 December 2025; Published: 03 April 2026

ABSTRACT: To meet the needs of the treatment of Cu^{2+} pollution in aqueous solution, the sodium alginate-modified polyacrylic acid (PAA/SA) composite hydrogel was prepared by solution polymerization with acrylic acid (AA) as monomer, sodium alginate (SA) as filler, N, N'-methylenebisacrylamide (MBA) as crosslinking agent, and potassium persulfate ($K_2S_2O_8$) as initiator. The characterization results showed that the introduction of SA significantly improved the physical and chemical properties of PAA hydrogel materials. Scanning electron microscopy (SEM) showed that as the SA content increased, the materials gradually evolved from a dense blocky structure to a porous network. When the SA content was 10 wt%, it exhibited a fragmented layered morphology. The Brunauer Emmett Teller (BET) showed that the specific surface area reached 37.65 m^2/g and the porosity increased to 12.47%. Fourier transform infrared (FT-IR) spectroscopy confirmed that SA was successfully embedded into the PAA network through hydrogen bonding and ion crosslinking, and the carboxyl vibration peak shifted from 2378 to 2352 cm^{-1}. Mechanical tests showed that at 10 wt% SA, the maximum stress was 13.1 kPa. The adsorption experiment showed that the equilibrium adsorption capacity of the PAA/SA hydrogel for Cu^{2+} was 11.03 mg/g, with an adsorption efficiency of 42.65%. Dynamics studies showed that the adsorption process follows a first-order kinetic model (R^2 = 0.986–0.997), indicating a physical adsorption mechanism dominated by liquid film diffusion. The optimal process conditions were found to be a dosage of 1.5 g/L, and the effect of temperature on adsorption was limited. The material maintained 67.4% of its initial adsorption capacity after six adsorption-desorption cycles. These parameters are generally superior to those of similar materials reported in the literature, indicating broad application prospects. Such a kinetic and isotherm model resulted from the combined effects of functional groups, electrostatic attraction, and chelation. In practical applications, pH, ionic strength, and competing ions will affect the adsorption performance of PAA/SA composite hydrogels.

KEYWORDS: Polyacrylic acid (PAA) hydrogel; sodium alginate (SA); solution polymerization; copper ions; adsorption kinetics; adsorption isotherm

1 Introduction

With the acceleration of industrialization and urbanization, heavy metal pollution in soil and water has become a global environmental problem. Copper ions (Cu^{2+}), as a typical heavy metal pollutant, are widely present in industrial wastewater from industries such as electroplating, mining, and electronic manufacturing. They enter the human body through the food chain and bioaccumulation. Scientific research has shown that excessive intake of copper can cause liver and kidney damage, damage the nervous system, and even pose a risk of cancer [1–3]. According to China's Comprehensive Wastewater Discharge Standard (GB8978-1996), the allowable discharge limit for Cu^{2+} varies by industry and discharge standard. For

example, the discharge limit for Cu^{2+} in general industrial wastewater is 0.5, 0.3 mg/L in the electroplating industry, and 0.82 mg/L in some chemical companies.

Although traditional treatment methods such as chemical precipitation, ion exchange, and membrane separation have certain effects, they face bottlenecks such as high cost, complex operation, and the easy generation of secondary pollution. For example, chemical precipitation requires high chemical doses, and the resulting sludge requires further treatment. Ion exchange has low removal efficiency for low-concentration heavy metals and high maintenance costs [4,5]. Therefore, the development of new, efficient, economical, and environmentally friendly adsorption materials has become a research hotspot in water pollution control. Hydrogel materials show excellent adsorption properties due to their three-dimensional network structure, high porosity, and rich functional groups [6–8]. Among them, polyacrylic acid (PAA) hydrogels have been widely studied due to their strong coordination ability of carboxyl groups with heavy metal ions. However, their drawbacks, such as low mechanical strength and poor swelling stability, limit their widespread application [9–11]. Sodium alginate (SA) is a natural anionic polysaccharide with biodegradability, non-toxicity, and strong ion exchange ability. Therefore, the SA-PAA complex can exhibit a synergistic effect through physical/chemical crosslinking, significantly improving the adsorption capacity and structural stability of the composite hydrogel [12,13].

In recent years, significant progress has been made in the research of chitosan- and SA-modified hydrogels at home and abroad. For example, Li et al. [14] created a PAA/chitosan hydrogel, which selectively adsorbed Cu^{2+} through carboxyl-amino chemical crosslinking, proving that the maximum adsorption capacity of the Langmuir model was 99.1 mg/g. When coexisting with Cd^{2+}, the material exhibited high selectivity with a selectivity coefficient of 3.3. Wang and You [15] prepared Cu^{2+}-imprinted crosslinked chitosan resin microspheres via ion-imprinting technology, using chitosan as the matrix and epichlorohydrin as the crosslinking agent. The adsorption process followed quasi-two-stage kinetics and the Langmuir isotherm model, mainly controlled by surface-adsorption, achieving an optimal adsorption capacity of 95.2 mg/g. Zhao [16] developed a polyvinyl alcohol (PVA)/SA composite hydrogel via graft copolymerization and achieved a Cu^{2+} adsorption capacity of 98.7 mg/g through its crosslinking network, which was 1.8 times higher than that of the pure PVA hydrogel. Meng et al. [17] used dopamine-modified polyacrylamide (PAM)/SA hydrogel to significantly improve the adsorption performance of Cu^{2+}. Due to the catechol group of dopamine, the modified hydrogel showed enhanced metal chelating ability, with an adsorption capacity of 49.8 mg/g for Cu^{2+}, and maintained more than 90% activity after five adsorption-desorption cycles. Kong et al. [18] fabricated a GO/PAA/SA triple-network hydrogel in which the oxygenated groups of GO and the carboxylates of SA act as paired ligands; this synergistic chelation markedly enhances ion binding, enabling selective removal of Cd^{2+} and Cu^{2+} with a Langmuir Cd^{2+} capacity of 268 mg g^{-1}. Guo et al. [19] synthesized PAA/SA-based titanium dioxide (TiO_2) composite material (PAA/SA@TiO_2) hydrogel, and evaluated its ammonia nitrogen adsorption efficiency. Under optimal conditions (6 g/L adsorbent and pH 7), the adsorption efficiency of Langmuir monolayer adsorption kinetics for ammonia nitrogen pollutants with concentrations of 100, 200, and 300 mg/L at 35°C adsorption temperature and 70 min equilibrium time were 85.56%, 79.46%, and 67.63%, respectively, which was consistent with pseudo-second order kinetics. Tally and Atassi [20] synthesized PAA/SA superabsorbent hydrogel through microwave-assisted synthesis, revealing the compliance of the Langmuir model. Their pH-sensitive properties caused them to contract under acidic conditions to expose adsorption sites, and then expand under alkaline conditions to release metal ions, thereby optimizing the adsorption-desorption cycle efficiency. This reversible structural change mechanism was crucial for the regeneration of adsorbents, a key factor in their practical application for heavy metal recovery, as emphasized in the previous review [21].

Despite these advances, there are still many shortcomings in the performance and adsorption mechanism of these materials for Cu^{2+} pollutants, which seriously hinder their practical applications. Therefore, it is necessary to further carry out some in-depth and systematic work in these fields. In this study, the SA-modified PAA (PAA/SA) composite hydrogel will be prepared by solution polymerization with acrylic acid (AA) as monomer, SA as filler, N,N'-methylenebisacrylamide (MBA) as crosslinking agent, and potassium persulfate ($K_2S_2O_8$) as initiator. The adsorption performance of Cu^{2+} was systematically evaluated by adjusting the amount of SA and PAA hydrogels, the initial concentration, and temperature of Cu^{2+}. Through these works, we hope to provide a theoretical basis and practical guidance for the composition and structural design of related material systems and their practical applications.

2 Experimental Section

2.1 Experimental Raw Materials

SA and AA with a purity ≥99.0% were purchased from Dalian Hefu Trading Co., Ltd., China; MBA with a purity ≥99.5% was supplied by Zibo Minghui Petrochemical Co., Ltd., China; $K_2S_2O_8$ with a purity ≥99.0% and copper nitrate ($Cu(NO_3)_2$) with a purity ≥99.0% were provided by Wuxi Prospect Chemical Reagent Company, China.

2.2 Experimental Equipment

The equipment included a magnetic stirrer (IKA RH Digital, Germany), a constant temperature water bath (DK-98-II, Shanghai Jinghong Experimental Equipment Co., Ltd., China) with a temperature control range from ambient temperature to 100°C and a temperature control accuracy 0.1°C, a freeze dryer (FreeZone 2.5 L, Labconco, USA), an inductively coupled plasma emission spectrometer (ICP-OES, iCAP 7400, Thermo Fisher Scientific, USA), a centrifuge (Eppendorf 5424, Eppendorf, Germany), a Fourier transform infrared spectrometer (FT-IR, Nicolet iS10, Thermo Scientific, USA), a scanning electron microscope (SEM, SU8010, Hitachi, Japan), a universal material testing machine (Instron 5960, Instron, USA), and a specific surface area and pore size analyzer (ASAP 2460, Micromeritics, USA).

2.3 Preparation of SA-Modified PAA Hydrogel

2.3.1 Preparation Process of PAA/SA Composite Hydrogel

Scheme 1 shows the preparation flow chart of the PAA/SA composite hydrogel. The detailed procedure is as follows.

(1) Preparation of SA Solution

Various masses of 0.1, 0.5, and 1.0 g of SA powder were weighed and added to 10 mL of deionized water maintained in a constant-temperature water bath at 60°C. These solutions with 1, 5, and 10 wt% SA were stirred continuously until SA was completely dissolved, yielding transparent, viscous solutions of different concentrations.

(2) Monomer Mixture and Crosslinking System

An AA monomer of 1.0 g was weighed and added to the SA solution, which was stirred for 10 min to obtain a homogeneous mixture. Subsequently, 0.02 g of MBA as a crosslinking agent and 0.02 g of $K_2S_2O_8$ as an initiator were added, and the mixture was continuously stirred at 30°C until all solids were completely dissolved, forming a precursor solution.

(3) Polymerization Reaction

The precursor solution was transferred to a sealed glass container, and high-purity nitrogen (≥99.99%) was introduced for 15 min to eliminate dissolved oxygen and suppress side reactions during

free radical polymerization. Subsequently, the container was sealed and incubated in a 70°C water bath for 7 h to complete the free-radical polymerization of AA monomers and the crosslinking of the PAA/SA networks.

(4) Post-Treatment of Hydrogel

After the reaction was completed, the hydrogel sample was placed in a refrigerator for at least 24 h. Then the frozen hydrogel was placed in a freeze-dryer and vacuum-dried at −50°C for 168 h to produce porous dried hydrogel samples for subsequent adsorption tests.

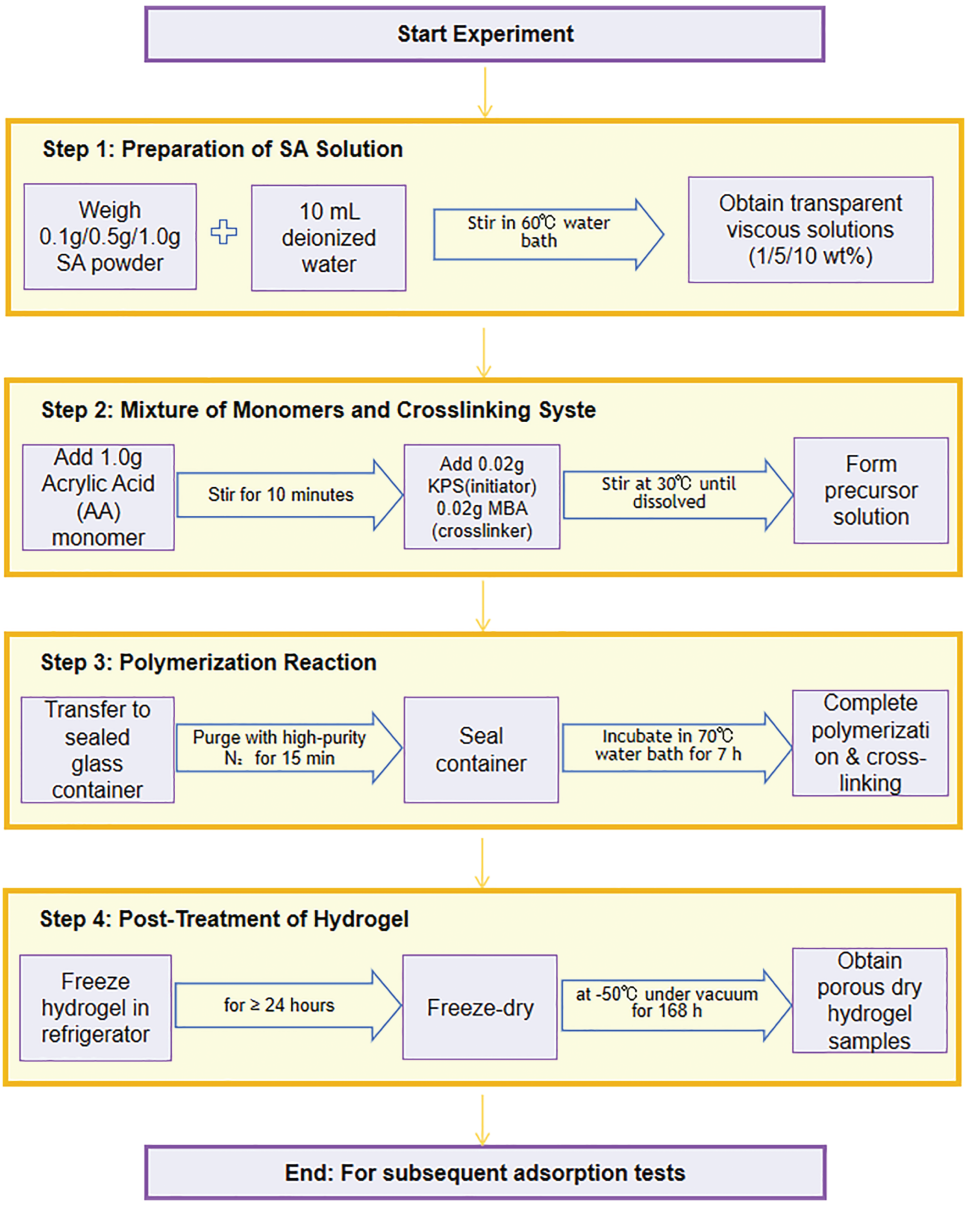

Scheme 1: Preparation flow chart of PAA/SA composite hydrogel

2.3.2 Preparation of Pure PAA Hydrogel

The pure PAA hydrogel without SA modification was also prepared by the same synthesis process as the control sample. The specific procedure included dissolving 1.0 g of AA in 10 mL of deionized water, then

adding 1.0 mol% MBA and 0.5 mol% $K_2S_2O_8$. After stirring to form a homogeneous solution, the sample was processed according to the same standard protocol, including nitrogen degassing, 70°C water bath polymerization, and post-treatment procedures.

2.4 Characterization of SA-Modified PAA Hydrogel

2.4.1 Comparative Test on the Adsorption Performance of Hydrogels with Different SA Content

A 250 mL aqueous solution of $Cu(NO_3)_2$ at 50 mg/L was prepared and adjusted to pH 5.0. The same mass of 0.5 g of freeze-dried hydrogel with different SA contents (0, 1, 5, and 10 wt%) was weighed and added to the solution, which was then magnetically stirred at 25°C. The same volume (1 mL) of solution was collected at predetermined time points (5, 10, 20, 40, 60, 90, 120, 150, 180, 240, and 300 min) and then filtered through 0.22 μm membranes. The Cu^{2+} concentrations were measured using an inductively coupled plasma emission spectrometer. The adsorption efficiency (R_t) and adsorbed amount (q_t) were calculated using the following formulas, respectively:

$$R_t = \frac{C_0 - C_t}{C_0} \times 100\% \tag{1}$$

$$q_t = (C_0 - C_t)V \tag{2}$$

where, C_0 was the initial concentration, C_t was the concentration at time t, and V was the volume of the solution. The adsorption process was fitted by the first-order kinetic model (Formula (3)) and the second-order kinetic model (Formula (4)):

$$\ln(q_e - q_t) = \ln q_e - k_1 t \tag{3}$$

$$\frac{t}{q_t} = \frac{1}{k_2 q_e^2} + \frac{t}{q_e} \tag{4}$$

The adsorption efficiency-time and adsorption amount-time curves were plotted to compare the kinetic differences of hydrogels with different SA contents.

2.4.2 Effect of Hydrogel Dose Tests

The SA content was fixed to be 10 wt%, and the initial concentration of Cu^{2+} was 50 mg/L. Various masses of 0.2, 0.5, 1.0, 1.5, and 2.0 g of dry hydrogels were added, respectively, and the adsorption tests were carried out according to the above method. The influence of dosage on the adsorption equilibrium time and maximum adsorption capacity was analyzed.

2.4.3 Effect of Initial Concentration of Cu^{2+} Solution

With a 10 wt% SA-modified hydrogel (dose of 1.5 g), the adsorption behaviors of Cu^{2+} solutions with initial concentrations of 10, 20, 50, 80, and 100 mg/L, respectively, were tested. The equilibrium adsorption data were analyzed using Langmuir (Formula (5)) and the Freundlich (Formula (6)) isothermal models to evaluate the adsorption mechanisms:

$$\frac{C_e}{q_e} = b\frac{1}{q_{max}} + \frac{C_e}{q_{max}} \tag{5}$$

$$\ln q_e = \ln K_F - \ln C_e/n \tag{6}$$

where, q_{max} was the theoretical maximum adsorption capacity, b was the Langmuir constant, and K_F and n were the Freundlich constants.

2.4.4 Fourier Transform Infrared (FT-IR) Spectroscopy Analysis

An FT-IR spectrometer was employed using the KBr pellet method (sample: KBr = 1:100 (wt:wt)). The scan range was set between 4000 and 400 cm^{-1} with a resolution of 4 cm^{-1}. The characteristic shifts of the carboxyl, hydroxyl, and amide bonds in PAA after SA introduction were analyzed.

2.4.5 Scanning Electron Microscopy (SEM) Observation

The microscopic morphology of the hydrogel was observed using an SEM. After spraying gold onto the freeze-dried samples, surface and cross-sectional images were taken at an acceleration voltage of 5 kV.

2.4.6 Mechanical Property Test

The compression and tensile properties of the hydrogel were measured by a universal material testing machine.

(1) Compression Tests: The cylindrical gel specimens with a diameter of 10 and 5 mm in height were compressed at a rate of 1 mm/min to 80% strain, and the stress-strain curve was recorded.
(2) Tensile Tests: The dumbbell-shaped specimens following the ASTM D638 standard were stretched at a rate of 10 mm/min until fracture, and the tensile strength and elongation at break were measured.

2.4.7 Specific Surface Area and Pore Structure Analysis by BET Measurements

The hydrogels' specific surface area and pore-size distribution were measured using a specific surface area and pore-size analyzer via nitrogen adsorption-desorption. Prior to testing, the samples underwent 6-h vacuum degassing at 150°C. The nitrogen adsorption-desorption tests were conducted at a liquid nitrogen temperature of 77 K, with a relative pressure (p/p_0) range of 0.01–0.99. The specific surface area was calculated using the BET equation, while the pore size distribution and pore volume were determined by the Barrett-Joyner-Halenda (BJH) method. The pore structure types were classified according to the IUPAC classification standards.

2.4.8 Porosity Determination

The porosity of the hydrogel was determined using the liquid displacement method. The dried hydrogel sample with a weight of W_0 was immersed in n-hexane for 24 h until saturated, and the wet weight (W_1) was measured. The porosity (P) was calculated as follows:

$$P\,(\%) = \frac{W_1 - W_0}{\rho V} \times 100\% \tag{7}$$

where, ρ was the density of n-hexane (0.66 g/cm^3), and V was the volume of the hydrogel.

2.4.9 Adsorption-Desorption Cycle Test

To evaluate the regeneration performance and stability of the PAA/SA composite hydrogel, six adsorption-desorption cycles were conducted. The adsorption conditions were an initial Cu^{2+} concentration of 50 mg/L, pH 5.0, a temperature of 25°C, and an adsorption duration of 5 h. For the desorption process, the saturated hydrogel was transferred to a 0.1 mol/L HCl solution and stirred at 25°C for 2 h to achieve

the complete desorption. The desorbed hydrogel was washed with deionized water until neutralized, then freeze-dried for reuse in subsequent adsorption cycles. The adsorption efficiency and cyclic regeneration rate for each cycle were calculated as follows:

$$\text{Cyclic regeneration rate}\ (\%) = \frac{\text{Last adsorption capacity}}{\text{First adsorption capacity}} \times 100\% \tag{8}$$

2.4.10 Correlation Analysis between Mechanical Properties and Adsorption Properties

To investigate the effect of mechanical properties on adsorption performance, mechanical and adsorption tests were conducted simultaneously on hydrogels with the same SA concentration. The relationships between the compression modulus and tensile strength, and the Cu^{2+} adsorption capacity, were evaluated using correlation analysis. Pearson's correlation coefficient was used to assess the relationship between mechanical and adsorption parameters.

2.4.11 Effect of Temperature on Adsorption Performance

Under the experimental conditions of 35°C, 45°C, 55°C, 65°C, and 75°C, the effect of temperature on the Cu^{2+} adsorption by PAA/SA composite hydrogels was investigated. Other experimental parameters included an initial Cu^{2+} concentration of 50 mg/L, pH 5.0, and an adsorbent dosage of 1.5 g/L. The thermodynamic parameters, including Gibbs free energy ΔG, enthalpy change ΔH, and entropy change ΔS were analyzed to evaluate the spontaneity and endothermic/extothermic characteristics of the adsorption process.

3 Results and Discussion

3.1 Physical and Chemical Properties of PAA/SA Composite Hydrogel

3.1.1 Microstructure

SEM images of the PAA/SA composite hydrogels with different SA contents are shown in Fig. 1. It can be seen that the addition of SA significantly modulates the microstructure of PAA hydrogel. The pure PAA hydrogel without SA (Fig. 1d) exhibits a smooth, homogeneous surface, a dense bulk structure, and minimal microcracks. When 1 wt% SA is added (Fig. 1a), the gel surface develops irregular wrinkles and sparse pores with poor inter-pore connectivity. At 5 wt% SA (Fig. 1b), the number of pores increases markedly, forming a well-connected honeycomb network, indicating enhanced crosslinking density of PAA. Upon increasing SA content to 10 wt% (Fig. 1c), the material shows a fragmented layered morphology with significantly increased surface roughness, primarily due to the self-aggregation tendency of high-concentration SA chains and the competitive crosslinking effects with the PAA network. It could be the SA's carboxyl and hydroxyl groups, coupled with the PAA network through hydrogen bonding and ionic crosslinking, that significantly enhance the PAA hydrogel's heterogeneous nucleation capability [22].

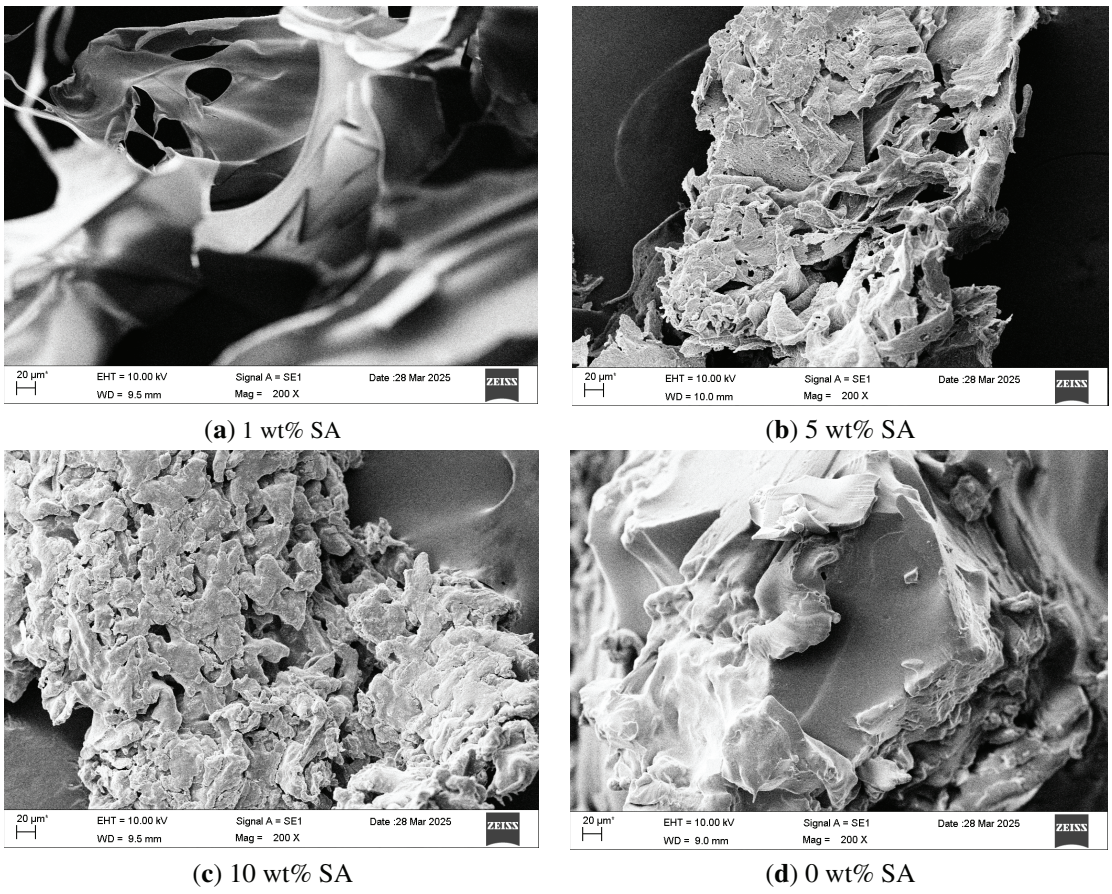

(**a**) 1 wt% SA (**b**) 5 wt% SA

(**c**) 10 wt% SA (**d**) 0 wt% SA

Figure 1: SEM images of PAA hydrogels with different SA contents: (**a**) 1 wt%, (**b**) 5 wt%, (**c**) 10 wt%, and (**d**) 0 wt%

3.1.2 Porous Structure

The hydrogel samples with different SA contents (1, 5, and 10 wt%) were characterized by nitrogen adsorption-desorption. As shown in Fig. 2, the BET test results reveal that all three materials exhibit the typical Type IV isotherm characteristics, accompanied by H3-type hysteresis loops [23]. This feature indicates the presence of a multi-level porous structure containing micropores, mesopores, and macropores. Pore-size distribution analysis further confirms the presence of mesoporous structures, with average pore sizes ranging from 2.72 to 3.82 nm across all three materials. This pore size range facilitates the diffusion-mass transfer of Cu^{2+} ions and ensures adequate exposure of adsorption sites.

The results show that the specific surface area of the hydrogel material with 10 wt% SA reaches 37.65 m^2/g, which is significantly higher than that of the samples with 1 and 5 wt% SA. The larger specific surface area provides more active adsorption sites for Cu^{2+} ions, thus improving the adsorption capacity [24].

The porosity analysis results (Fig. 3) indicate that as the SA content increases from 1 to 10 wt%, the hydrogel's porosity rises from 10.67% to 11.12% and 12.47%, respectively. The hydrogel with 10 wt% SA exhibits the highest porosity, providing abundant attachment sites for heavy metal ions and establishing an effective mass-transfer channel network that facilitates rapid diffusion and deep adsorption of Cu^{2+} ions within the hydrogel [25]. By adjusting key parameters such as pore structure, specific surface area, and porosity after SA addition, the material's Cu^{2+} adsorption performance can be significantly enhanced.

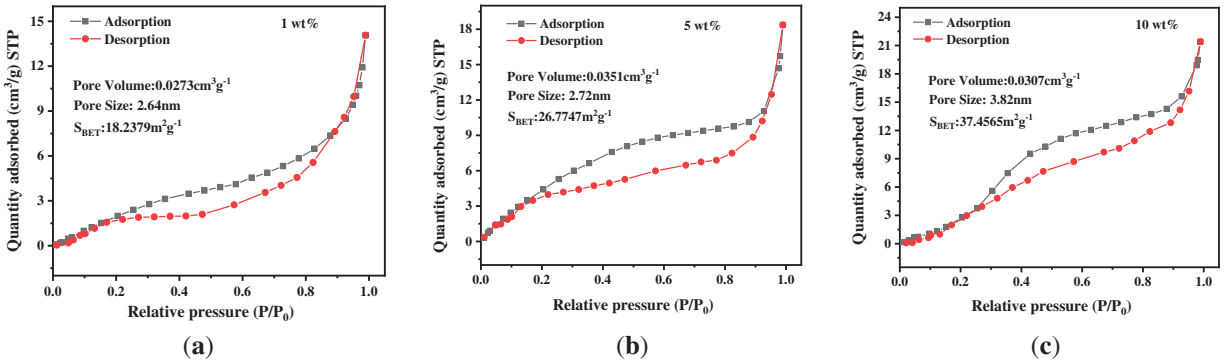

Figure 2: BET test curves of PAA/SA composite hydrogels with different SA contents: (**a**) 1 wt%, (**b**) 5 wt%, and (**c**) 10 wt%

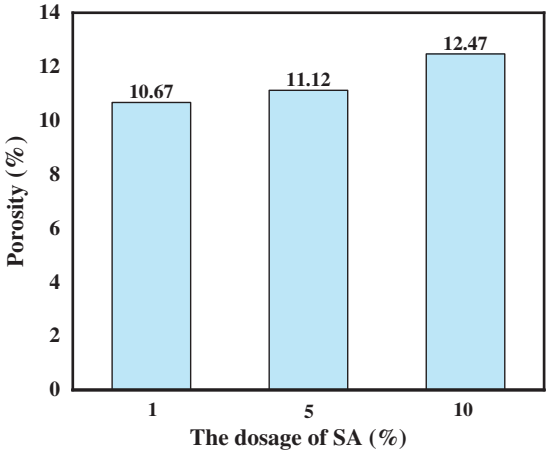

Figure 3: Porosity results of PAA/SA composite hydrogels with different SA contents

3.1.3 Functional Group Evolution and Chemical Interactions

The FTIR spectra (Fig. 4) reveal that the introduction of SA significantly alters the functional group characteristics of the hydrogels. The pure PAA hydrogel exhibits a broad peak at 3200–3600 cm^{-1}, attributed to the O-H stretching vibrations of carboxyl groups (-COOH) in AA and the association effect of intermolecular hydrogen bonds. After adding 10 wt% SA, this peak shifts to lower frequencies (approximately 3400–2900 cm^{-1}) and shows reduced broadening. This may be due to the formation of hydrogen bond interactions between SA's abundant hydroxyl groups (-OH) and PAA's carboxyl groups, stabilizing the three-dimensional structure of the composite hydrogel [26]. SA also modifies PAA's self-aggregation behavior, as its polysaccharide segments act as "intermolecular spacers" within the PAA network. The rigid sugar ring structure prevents excessive coiling and collapse of PAA chains, consistent with the honeycomb-like porous structure observed above in Section 3.1.1. In the carboxylate characteristic region (2300–2400 cm^{-1}), the control group shows a typical asymmetric stretching vibration peak at 2378 cm^{-1} for carboxylate groups (-COO-), indicating partial dissociation under neutral conditions. After the SA addition, this peak intensifies and shifts to lower wavenumbers (2352 cm^{-1}), with a faint shoulder peak observed at 2420 cm^{-1} (indicating incomplete neutralization of carboxyl C=O vibrations). This suggests that SA's carboxyl groups form a heterogeneous network structure with PAA carboxylates through hydrogen bonding or ionic crosslinking. This heterogeneity results in phase separation. The alternating distribution of SA-rich and PAA-rich regions creates interfacial voids, enhancing the material's porosity [27]. As shown in the figure, the characteristic

C-O-C (sugar ring ether bond) absorption peak at 1135 cm^{-1} of SA remains clearly visible in the composite sample, confirming successful integration of SA's polysaccharide backbone into the PAA hydrogel matrix. The rigid sugar ring structure of the SA molecular chains acts as a supporting framework, maintaining network openness during gelation. This rigidity-support effect shows high consistency with the above BET test results [28].

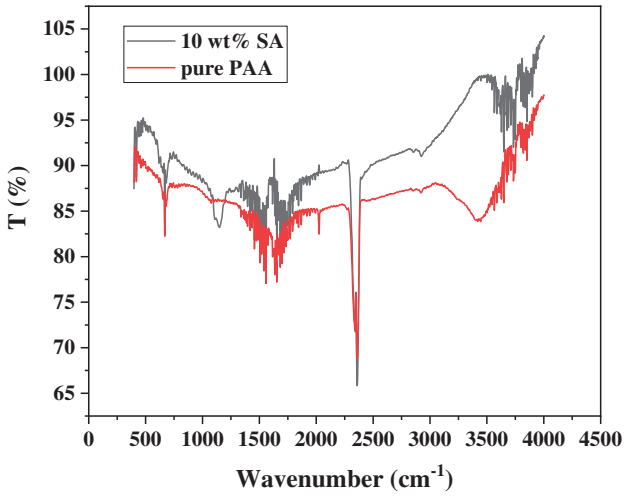

Figure 4: FTIR spectra of PAA/SA composite and pure PAA hydrogels

3.1.4 Mechanical Properties

Fig. 5 presents the stress-strain curves of PAA/SA composite hydrogels with varying SA contents. The pure PAA hydrogel exhibits typical soft-hydrogel characteristics at low strains, reaching a maximum stress of 3.25 kPa at 300% strain, indicating a lower crosslinking density and greater ductility in its network. After SA is added, the mechanical behavior of the PAA/SA composite hydrogels undergoes significant changes. With 5 wt% SA, the maximum stress increases to 9.51 kPa at 460% strain, attributed to the additional physical crosslinking points formed between SA's carboxyl groups and PAA networks, enhancing the crosslinked structure [29]. When the SA content reaches 10 wt%, the material demonstrates optimal performance, with the maximum stress rising to 13.1 kPa at 790% strain, representing 300% and 163% increases in stress and strain, respectively, compared to pure PAA. Moderate SA addition not only strengthens the three-dimensional network structure through ionic crosslinks and hydrogen bonding but also maintains excellent energy dissipation capability [30].

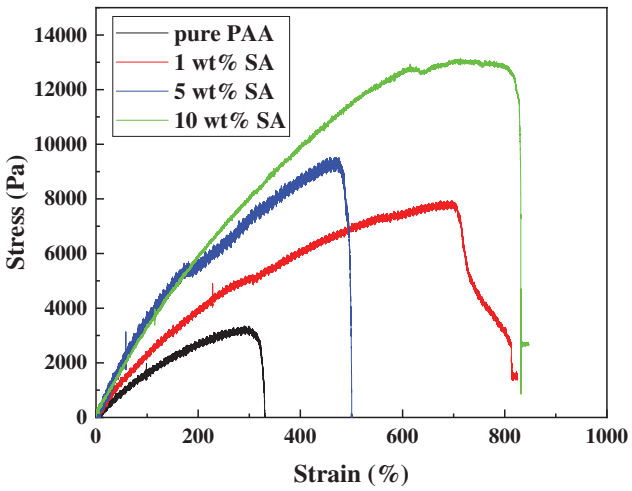

Figure 5: Mechanical properties of PAA/SA composite hydrogels with different SA contents

3.1.5 Correlation Analysis between Mechanical Properties and Adsorption Performance

The mechanical enhancement significantly boosts the Cu^{2+} adsorption capacity of PAA/SA composite hydrogels. As shown in Table 1, the hydrogel's compression modulus, tensile strength, and Cu^{2+} adsorption capacity all show a synchronous improvement trend with increasing SA content. At 10 wt% SA content, the material achieves a compression modulus of 4.37 kPa and tensile strength of 13.1 kPa, and its equilibrium adsorption capacity for Cu^{2+} increases to 11.03 mg/g, representing a 28.6% enhancement compared to the 8.58 mg/g for pure PAA hydrogel. This positive correlation (Pearson correlation coefficient R = 0.96) reveals an intrinsic connection between the mechanical reinforcement and the adsorption performance [31]. The enhanced mechanical strength ensures a stable three-dimensional network during adsorption, preventing structural collapse and loss of adsorption sites due to excessive swelling. Moderate rigidity maintains open channels, reducing mass transfer resistance for Cu^{2+} ions to fully contact internal adsorption sites. Meanwhile, excellent mechanical toughness endows the material with "rigid-flexible" characteristics, resisting external damage while promoting ion-functional group coordination through segmental motion, achieving integrated structural-function design.

Table 1: Mechanical properties and adsorption performance parameters of PAA/SA composite hydrogels with different SA contents

SA content (wt%)	Compression modulus (kPa)	Tensile strength (kPa)	Maximum strain (%)	Cu^{2+} equilibrium adsorption capacity (mg/g)	Adsorption efficiency (%)
0	1.08 ± 0.12	3.25 ± 0.21	300 ± 15	8.58 ± 0.32	34.11 ± 1.28
1	1.95 ± 0.18	5.82 ± 0.35	420 ± 22	9.24 ± 0.41	36.78 ± 1.63
5	3.16 ± 0.25	9.51 ± 0.48	460 ± 28	10.12 ± 0.38	39.84 ± 1.51
10	4.37 ± 0.31	13.10 ± 0.56	790 ± 35	11.03 ± 0.45	42.65 ± 1.74

3.2 Adsorption Performance of SA-Modified PAA Hydrogel on Cu^{2+} in Water

3.2.1 Comparison of Adsorption Performance of Hydrogel with Different SA Content

Fig. 6 demonstrates the adsorption performance and kinetic fitting results of Cu^{2+} in aqueous solution by PAA/SA composite hydrogels with different SA contents. Fig. 6a,b reveals that as SA content increases from 0 to 10 wt%, the equilibrium adsorption capacity rises from 8.58 to 11.03 mg/g, with adsorption efficiency improving from 34.11% to 42.65%. The kinetic model analysis shows that the first-order model yields higher R^2 values (0.986–0.997) than the second-order model (0.962–0.983) for pure PAA hydrogel, indicating that PAA/SA composite hydrogels predominantly follow first-order kinetics, which are dominated by physical adsorption mechanisms. This suggests that the Cu^{2+} diffusion from solution to material surfaces primarily controls the adsorption rate, while the second-order model's chemical adsorption assumption contributes minimally in these samples, probably due to the dynamic hydrogen bonds and ionic crosslinking structures within the PAA/SA networks—these weak interactions provide limited adsorption sites and fail to form stable chemical bonds. The strong correlation between the experimental results and the first-order kinetic fit further supports the presence of pronounced concentration-gradient-driven effects during adsorption, consistent with the exponential decay pattern observed under quasi-equilibrium conditions.

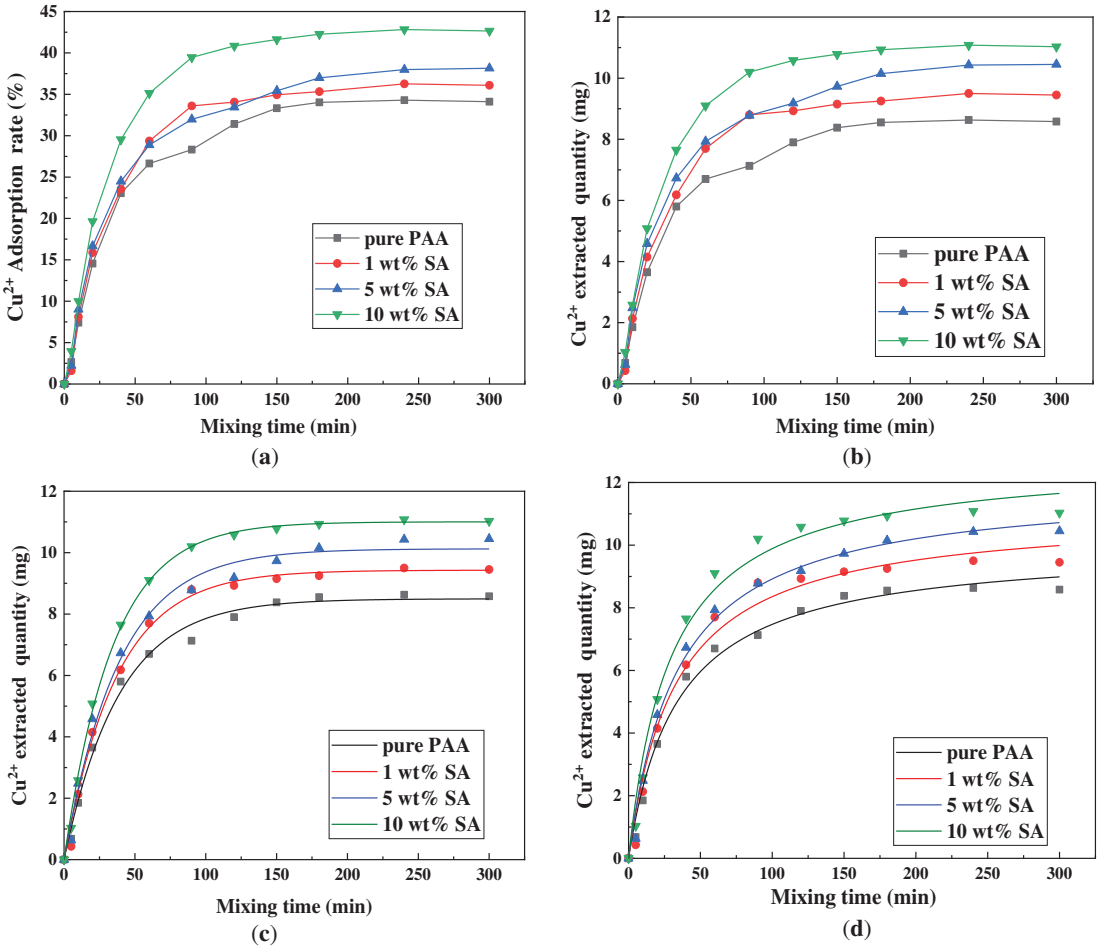

Figure 6: Comparison of adsorption performance of the PAA/SA composite hydrogels with different SA contents: (**a**) adsorption rate of Cu^{2+}, (**b**) the extracted amount of Cu^{2+}, (**c**) the first-order kinetic fitting of Cu^{2+} adsorption, and (**d**) the secondary kinetic fitting of Cu^{2+} adsorption

Table 2 compares the Cu^{2+} adsorption performance of our hydrogel materials with that reported in the literature. Our PAA/SA composite hydrogels exhibit higher maximum adsorption capacity.

Table 2: Comparison of the Cu^{2+} adsorption performance of our hydrogel materials with those in the literature

Researcher (Year)	Hydrogels	Adsorption object	Maximum adsorption capacity	Adsorption model
Li et al. (2019) [14]	PAA/Chitosan	Cu^{2+}	99.1 mg/g	Langmuir model; Chemical complexation (Amino and carboxyl groups)
Wang et al. (2021) [15]	Polyose resin/chitosan	Cu^{2+}	95.2 mg/g	Adsorption kinetics model and Langmuir adsorption isotherm model
Meng et al. (2023) [17]	PAM/SA (Dopamine modified)	Cu^{2+}	49.8 mg/g	Metal chelation (Catechol groups)
Zhao et al. (2021) [16]	PVA/SA	Cu^{2+}	98.7 mg/g	Langmuir model
This study	PAA/SA	Cu^{2+}	110.3 mg/g (Converted for comparison)	Langmuir isotherm adsorption model

3.2.2 Comparison of Adsorption Performance with Different Hydrogel Dosages

The effects of varying hydrogel dosages on the Cu^{2+} adsorption capacity of PAA/SA composite hydrogels are illustrated in Fig. 7. As the dosage increases from 0.2 to 1.5 g, the equilibrium adsorption rate rises from 31% to 51%. When it further increases to 2.0 g, the equilibrium adsorption rate decreases slightly from 51% to 47%, likely due to aggregation effects caused by the excess hydrogel, which masks some active sites. The analysis of the adsorption curves reveals a typical two-stage process: the first 160 min (rapid adsorption phase) is dominated by liquid-film diffusion, accounting for over 80% of the total adsorption capacity; followed by a slow equilibrium phase (slow diffusion phase) in the subsequent 180 min. When the dosage exceeds 1.5 g, the growth rate of adsorption efficiency per unit mass slows. The practical applications should therefore select an appropriate 1.0–1.5 g/L dosage based on the treatment scale and cost consideration.

3.2.3 Effect of Solution Cu^{2+} Concentration

Fig. 8 compares the adsorption performance and isothermal model-fitting results of PAA/SA composite hydrogels at different initial Cu^{2+} concentrations. As shown in Fig. 8a, the adsorption rate of Cu^{2+} decreases with increasing solution concentration. The PAA/SA composite hydrogels achieve a peak adsorption rate of 66.9% at an initial Cu^{2+} concentration of 10 mg/L, which drops to 34.7% at 100 mg/L. This phenomenon can be attributed to a higher contact probability between Cu^{2+} ions and adsorption sites at low concentrations, where carboxyl and hydroxyl groups on the hydrogel surface rapidly bind metal ions. However, at high concentrations, saturated adsorption sites reduce the available adsorption sites, intensifying competition among ions and consequently decreasing adsorption efficiency. Conversely, Fig. 8b shows a significant increase in equilibrium adsorption capacity (q_e) with rising Cu^{2+} concentration. At 10 mg/L, q_e reaches 1.9 mg/g, while it rises to 6.2 mg/g at 100 mg/L. This occurs because, although the total amount of Cu^{2+} in solution increases at higher concentrations, the absolute quantity per unit mass of hydrogel still shows a marked rise in metal adsorption, aligning with the concentration gradient-driven diffusion adsorption

principles. The analysis of the adsorption isothermal model shows that the correlation coefficient (R^2) of Langmuir model is between 0.993 and 0.998, which is significantly higher than that of Freundlich model (R^2 is between 0.922 and 0.957), indicating that the adsorption of Cu^{2+} by PAA/SA composite hydrogels is more consistent with the homogeneous adsorption mechanism of single layer, which is consistent with the ordered arrangement characteristics of SA carboxyl group in PAA/SA network.

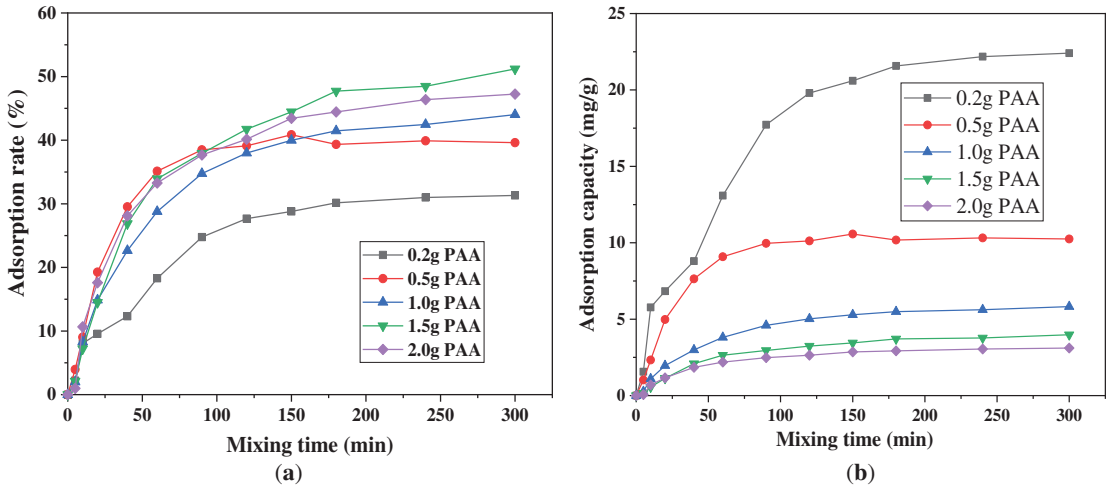

Figure 7: Comparison of PAA/SA composite hydrogel adsorption performance with different dosages: (**a**) adsorption rate and (**b**) adsorption capacity

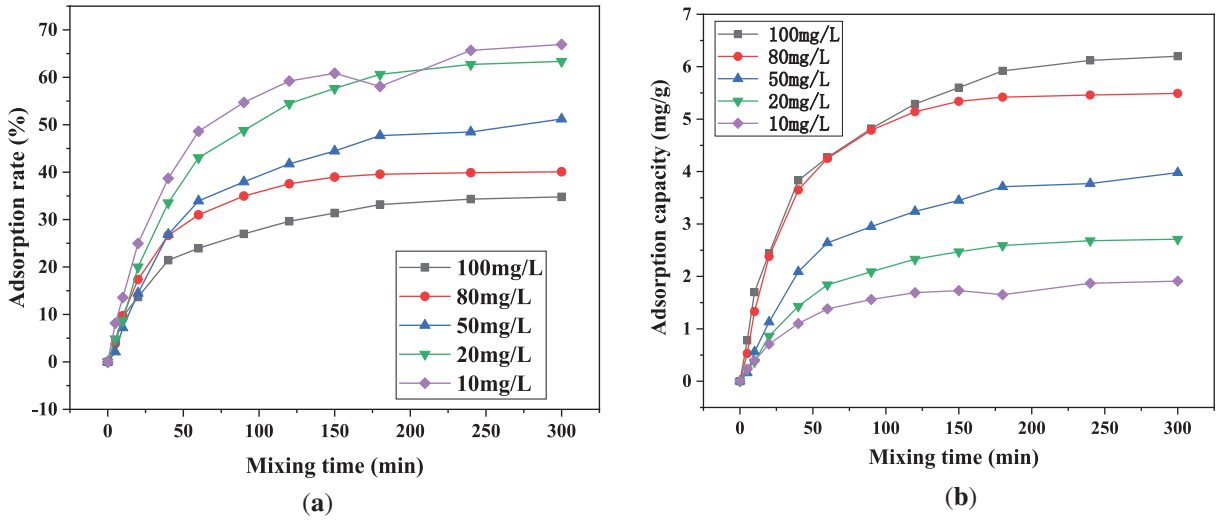

Figure 8: (Continued)

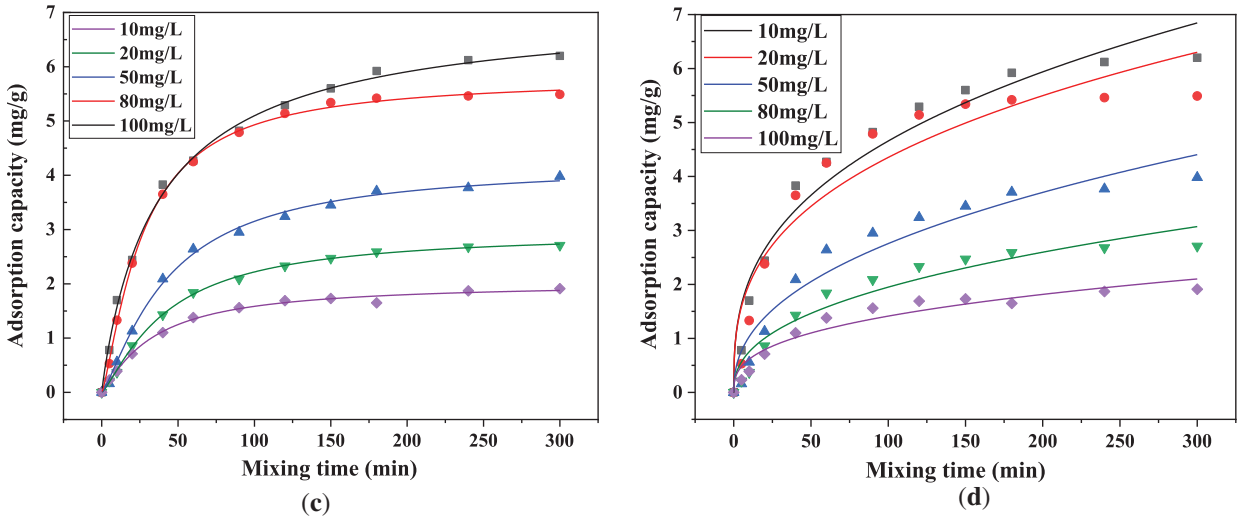

Figure 8: Comparison of the adsorption performance of PAA/SA composite hydrogels for different Cu^{2+} concentrations: (**a**) adsorption rate, (**b**) adsorption capacity, (**c**) Langmuir adsorption isotherm curve, and (**d**) Freundlich adsorption isotherm curve

3.2.4 Effect of Adsorption Temperature

Fig. 9 compares the adsorption kinetics of Cu^{2+} by PAA/SA composite hydrogels at different temperatures. The data clearly show that both the adsorption rate and capacity increase slightly with increasing temperature. At 35°C, the equilibrium adsorption rate reaches 49.3% with a q_e of 4.2 mg/g. When the temperature rises to 75°C, the adsorption rate increases to 55.7% with q_e reaching 5.0 mg/g. This demonstrates that elevated temperature enhances Cu^{2+} diffusion efficiency by increasing molecular thermal motion and moderately relaxes the three-dimensional network structure of PAA composite hydrogels, thereby facilitating contact between internal adsorption sites and metal ions in solution. Although the temperature increase improves adsorption performance (approximately 13% increase in adsorption rate and 19% increase in capacity), the relative magnitude of these improvements reflects the thermal stability of the PAA/SA composite hydrogels. The temperature effect is particularly pronounced. The adsorption rate accelerates significantly during the initial phase (0–30 min) at higher temperatures. At 35°C, the equilibrium takes 180 min to achieve, while at 75°C, it completes in just 90 min—a 50% reduction in equilibrium time. This is attributed to decreased solution viscosity and accelerated ion migration at higher temperatures, effectively shortening the diffusion time of Cu^{2+} from the solution bulk to the hydrogel surface and interior.

3.2.5 Adsorption-Desorption Cycles and Passivation Stability

To evaluate the regeneration performance of PAA/SA composite hydrogels and the long-term stability of Cu^{2+} passivation, six consecutive adsorption-desorption cycles were conducted on the PAA/SA composite hydrogel containing 10 wt% SA, as shown in Fig. 10. The initial adsorption rate reaches 43.3% at the first cycle. After desorption treatment with 0.1 mol/L HCl solution, the desorption rate reaches 95.6%, indicating that the protonation under acidic conditions effectively disrupts the coordination bond between Cu^{2+} and carboxyl groups, achieving efficient metal ion desorption. With increasing cycle number, the adsorption rate declines gradually: 40.8% at the second cycle (94.2% retention), 36.6% at the fourth cycle (84.5% retention), and 29.2% at the sixth cycle (67.4% retention). This performance degradation can be attributed to repeated acid washing, which causes partial detachment of SA segments from the PAA network and leads to the loss

of active sites; the repeated swelling-constriction cycles during adsorption-desorption also contribute to the partial collapse of pore structures. Despite the performance degradation, the material retains 67.4% of its initial adsorption capacity after six cycles, outperforming the pure PAA hydrogels reported in literature [11]. This demonstrates that SA not only enhances adsorption capacity but also improves structural stability through its rigid sugar ring, effectively delaying performance degradation during cyclic use.

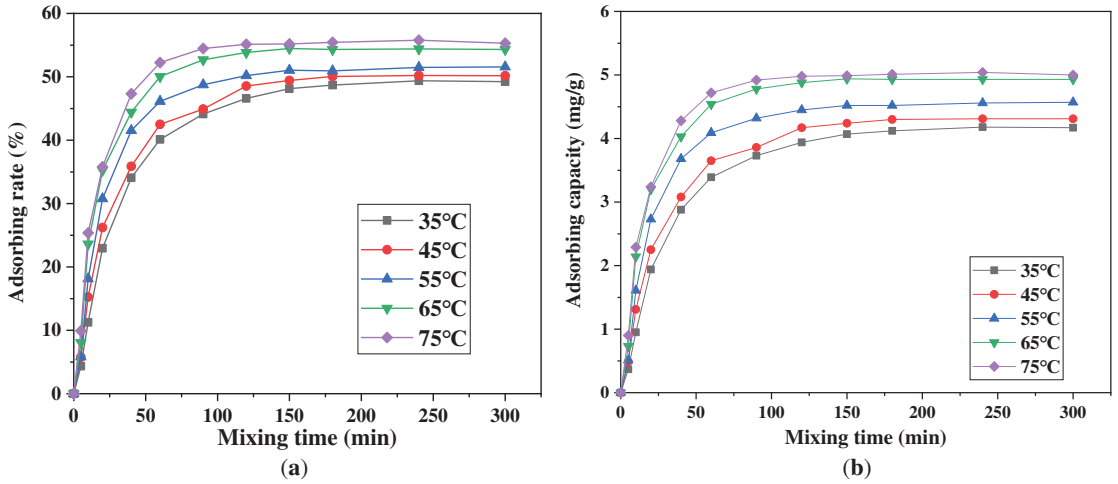

Figure 9: Comparison of the adsorption performance of PAA/SA composite hydrogels for Cu^{2+} at different temperatures: (**a**) adsorption rate, and (**b**) adsorption capacity

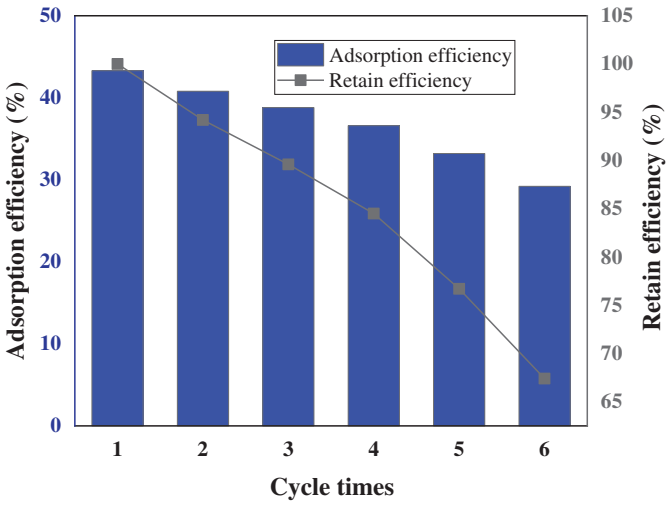

Figure 10: Experimental results of 6 consecutive adsorption-desorption cycles of PAA/SA composite hydrogels

4 Conclusions

PAA/SA composite hydrogel has been successfully prepared by solution polymerization, and its adsorption performance and mechanism for Cu^{2+} in water have been systematically studied. The following conclusion can be drawn:

(1) SEM analysis showed that with the increase of SA content, the material evolved from a dense block structure in pure PAA to a porous interconnected network, and a unique fragmented layered morphology was observed at 10 wt% SA. BET testing confirmed a specific surface area of 37.65 m^2/g and a porosity of 12.47%, providing abundant active sites and mass transfer channels for Cu^{2+} adsorption. In conclusion, the addition of SA significantly enhanced the microstructure and physicochemical properties of PAA hydrogels.

(2) When the dosage of SA was 10 wt%, the maximum stress reached 13.1 kPa, the strain reached 790%, the compressive modulus reached 4.37 kPa, and the tensile strength reached 13.1 kPa. There was a strong positive correlation between mechanical performance and adsorption capacity, as increased mechanical strength effectively maintained structural stability during adsorption. In summary, the addition of SA achieved a synergistic enhancement of mechanical and adsorption properties.

(3) The adsorption kinetics study showed that the adsorption of Cu^{2+} by PAA/SA composite hydrogel conformed to the first-order kinetic model ($R^2 > 0.986$), which confirmed that the liquid film diffusion was the rate-determining step. The adsorption process exhibited a clear two-stage characteristic: the initial 160 min rapid adsorption stage accounted for over 80% of the total adsorption capacity, while the subsequent 180 min slowed down the flow of the equilibrium phase. The isothermal adsorption conformed to the Langmuir model, indicating a uniform single-layer adsorption mechanism.

(4) When the SA dosage was 0.1 g, the equilibrium adsorption capacity reached 11.03 mg/g, and the adsorption efficiency was 42.65%. The optimal dosage was 1.5 g/L. Although the temperature increased from 35°C to 75°C, the adsorption rate increased by only 13%, while the equilibrium time decreased by 50%. In summary, the material exhibits excellent regeneration performance, maintaining 67.4% of its initial adsorption capacity after six cycles.

Regarding the limitations of this work, we still have shortcomings in accurately characterizing the chemical structure (functional groups) of SA and its interaction sites with PAA. In addition, we still lack a detailed understanding of the electrostatic interaction, chelation, and other processes in PAA/SA composite hydrogels. The influence of pH value, ion strength, competitive ions, etc., in actual wastewater on the actual adsorption performance of materials is also something we need to further understand.

In our further work, we can use the prepared PAA/SA composite hydrogel to adsorb Cu^{2+}-containing wastewater from different sources, assess its actual working capacity, and further optimize the material composition and structural design based on its performance.

Acknowledgement: Not applicable.

Funding Statement: This research was funded by Quality Engineering Project Fund of Anhui University of Applied Technology, grant numbers 2024xjjxyjy41 and 2024xjjpkc05.

Author Contributions: The authors confirm contribution to the paper as follows: Conceptualization: Hui Fan and Xinqiang Li; methodology: Hui Fan; software: Hui Fan; validation: Hui Fan and Xinqiang Li; formal analysis: Hui Fan and Xinqiang Li; investigation: Hui Fan; resources: Xinqiang Li; data curation: Xinqiang Li; writing—original draft preparation: Hui Fan; writing—review and editing: Hui Fan and Xinqiang Li; visualization: Hui Fan; supervision: Xinqiang Li; project administration: Hui Fan; funding acquisition: Hui Fan. All authors reviewed the results and approved the final version of the manuscript.

Availability of Data and Materials: Due to the nature of this research, participants of this study did not agree for their data to be shared publicly, so supporting data is not available.

Ethics Approval: Not applicable.

Conflicts of Interest: The authors declare no conflicts of interest to report regarding the present study.

References

1. Kamal KH, Hassan MA, Kamel S, El-Sayed NS. Efficient removal of Cd^{2+} ions and methylene blue from aqueous solutions by polyanionic sodium alginate-derived hydrogel. Surf Interfaces. 2024;51:104596. doi:10.1016/j.surfin.2024.104596.
2. Zhang L, Zeng Y, Cheng Z. Removal of heavy metal ions using chitosan and modified chitosan: a review. J Mol Liq. 2016;214:175–91. doi:10.1016/j.molliq.2015.12.013.
3. Wang Y. Adsorption-coupled electrophoretic remediation of heavy metal contaminated soils using graphene oxide hydrogel [dissertation]. Changchun, China: Jilin University; 2024. (In Chinese).
4. Hu ZH, Omer AM, Ouyang XK, Yu D. Fabrication of carboxylated cellulose nanocrystal/sodium alginate hydrogel beads for adsorption of Pb(II) from aqueous solution. Int J Biol Macromol. 2018;108(3):149–57. doi:10.1016/j.ijbiomac.2017.11.171.
5. Gkika DA, Mitropoulos AC, Kyzas GZ. Why reuse spent adsorbents? The latest challenges and limitations. Sci Total Environ. 2022;822:153612. doi:10.1016/j.scitotenv.2022.153612.
6. Ma D, Tao E, Yang S. Efficient removal of Cu(II) with graphene oxide-titanium dioxide/sodium alginate composite beads: preparation, characterization, and adsorption mechanism. J Environ Chem Eng. 2021;9(6):106501. doi:10.1016/j.jece.2021.106501.
7. Wang Y, Lu Y. Sodium alginate-based functional materials toward sustainable applications: water treatment and energy storage. Ind Eng Chem Res. 2023;62(29):11279–304. doi:10.1021/acs.iecr.3c01082.
8. Yadav MK, Saidulu D, Ghosal PS, Mukherjee A, Gupta AK. A review on the management of arsenic-laden spent adsorbent: insights of global practices, process criticality, and sustainable solutions. Environ Technol Innov. 2022;27:102500. doi:10.1016/j.eti.2022.102500.
9. Arafa EG, Mahmoud R, Gadelhak Y, Gawad OFA. Design, preparation, and performance of different adsorbents based on carboxymethyl chitosan/sodium alginate hydrogel beads for selective adsorption of Cadmium (II) and Chromium (III) metal ions. Int J Biol Macromol. 2024;273(1):132809. doi:10.1016/j.ijbiomac.2024.132809.
10. Kandil H, El-Wakeel ST. Effective removal of Pb(II) and Cu(II) from aqueous solutions using a hybrid composite of fuller's earth, aluminum silicate and chitosan. Polym Bull. 2024;81(2):1839–59. doi:10.1007/s00289-023-04792-8.
11. Zhang J, Qu D, Wang S, Qi S, Zuo H. Structure, property optimization, and adsorption properties of N,N′-methylenebisacrylamide crosslinked polyacrylic acid hydrogels under different curing conditions. Polymers. 2024;16(14):1990. doi:10.3390/polym16141990.
12. Liu S, Huang G. Experimental study on heavy metal Ion adsorption by natural zeolite in electroplating wastewater. Guangdong Chem Ind. 2022;49(23):162–4+142. (In Chinese).
13. Iamsaard K, Weng CH, Yen LT, Tzeng JH, Poonpakdee C, Lin YT. Adsorption of metal on pineapple leaf biochar: key affecting factors, mechanism identification, and regeneration evaluation. Bioresour Technol. 2022;344(Pt A):126131. doi:10.1016/j.biortech.2021.126131.
14. Li SS, Wang XL, An QD, Xiao ZY, Zhai SR, Cui L, et al. Upon designing carboxyl methylcellulose and chitosan-derived nanostructured sorbents for efficient removal of Cd(II) and Cr(VI) from water. Int J Biol Macromol. 2020;143(11):640–50. doi:10.1016/j.ijbiomac.2019.12.053.
15. Wang M, You XY. Critical review of magnetic polysaccharide-based adsorbents for water treatment: synthesis, application and regeneration. J Clean Prod. 2021;323(3):129118. doi:10.1016/j.jclepro.2021.129118.
16. Zhao D. Study on the adsorption behavior of heavy metals in water by modified sodium alginate composite hydroge [master's thesis]. Changchun, China: Jilin Agricultural University; 2021. (In Chinese).
17. Meng X, Yang S, Yu H, Zuo F. Preparation and properties of dopamine-modified sodium alginate/polyacrylamide hydrogel. J Southwest Minzu Univ. 2023;49(1):33–9. (In Chinese).
18. Kong W, Yue Q, Li Q, Gao B. Adsorption of Cd^{2+} on GO/PAA hydrogel and preliminary recycle to GO/PAA-CdS as efficient photocatalyst. Sci Total Environ. 2019;668:1165–74. doi:10.1016/j.scitotenv.2019.03.095.

19. Guo C, Han Y, Zhao W, Zhang X. Study on the adsorbing performance of ammonia nitrogen by polyacrylic acid-grafted sodium alginate-based titanium dioxide (PAASA@TiO_2) composite hydrogel. Environ Chem. 2024;43(7):2421–31. (In Chinese). doi:10.5004/dwt.2023.30208.
20. Tally M, Atassi Y. Synthesis and characterization of pH-sensitive superabsorbent hydrogels based on sodium alginate-g-poly(acrylic acid-co-acrylamide) obtained via an anionic surfactant micelle templating under microwave irradiation. Polym Bull. 2016;73(11):3183–3208. doi:10.1007/s00289-016-1649-8.
21. Lata S, Singh PK, Samadder SR. Regeneration of adsorbents and recovery of heavy metals: a review. Int J Environ Sci Technol. 2015;12(4):1461–78. doi:10.1007/s13762-014-0714-9.
22. Shi T, Xie Z, Zhu Z, Shi W, Liu Y, Liu M, et al. Effective removal of metal ions and cationic dyes from aqueous solution using different hydrazine-dopamine modified sodium alginate. Int J Biol Macromol. 2022;195(4):317–28. doi:10.1016/j.ijbiomac.2021.12.039.
23. Zhang W, Ou J, Wang B, Wang H, He Q, Song J, et al. Efficient heavy metal removal from water by alginate-based porous nanocomposite hydrogels: the enhanced removal mechanism and influencing factor insight. J Hazard Mater. 2021;418:126358. doi:10.1016/j.jhazmat.2021.126358.
24. Zhang H, Han X, Liu J, Wang M, Zhao T, Kang L, et al. Fabrication of modified alginate-based biocomposite hydrogel microspheres for efficient removal of heavy metal ions from water. Colloids Surf A Physicochem Eng Aspects. 2022;651(8):129736. doi:10.1016/j.colsurfa.2022.129736.
25. Zheng C, Wu Q, Sun K, Xu B, Sun Y, Zheng H. Insight into the impact of environmental factors on heavy metal adsorption by sodium alginate hydrogel: inspiration on applicable scenarios. Environ Res. 2024;262(4):119878. doi:10.1016/j.envres.2024.119878.
26. Feng Y, Sawut A, Simayi R, Maimaitiyiming X, Jiao X. *In situ* self-assembly of ZIF-8@sodium alginate composite hydrogels for enhanced adsorption of Cu^{2+} Ions. Colloids Surf A Physicochem Eng Aspects. 2024;702:135040. doi:10.1016/j.colsurfa.2024.135040.
27. Li J, Chen M, Yang X, Zhang L. Preparation of a novel hydrogel of sodium alginate using rural waste bone meal for efficient adsorption of heavy metals cadmium ion. Sci Total Environ. 2023;863:160969. doi:10.1016/j.scitotenv.2022.160969.
28. Lin Z, Yang Y, Liang Z, Zeng L, Zhang A. Preparation of chitosan/calcium alginate/bentonite composite hydrogel and its heavy metal ions adsorption properties. Polymers. 2021;13(11):1891. doi:10.3390/polym13111891.
29. Du M, Cao Y, Luo X, Yang W, Lin W, Wang Y, et al. Shapeable sodium alginate aerogel beads incorporated with L-cysteine-modified defective UiO-67 for heavy metal ions removal. Chem Eng J. 2023;475(1):146289. doi:10.1016/j.cej.2023.146289.
30. Yang C, Xu M, Wang Y, Li S, Lv X, Wang H, et al. Recyclable hydrogel-MOFs composite beads for selective removal of Pb(II) from water. Chem Eng Res Des. 2023;193(31):540–54. doi:10.1016/j.cherd.2023.03.052.
31. Wu X, Song Y, Yin P, Xu Q, Yang Z, Xu Y, et al. Fabrication of the composite sepiolite@polyethyleneimine/sodium alginate and its excellent adsorption performance for heavy metal ions. Appl Clay Sci. 2022;228(1):106647. doi:10.1016/j.clay.2022.106647.